Using high-resolution distributed temperature sensing to quantify spatial and temporal variability in vertical hyporheic flux

Martin A. Briggs,[1] Laura K. Lautz,[1] Jeffrey M. McKenzie,[2] Ryan P. Gordon,[1] and Danielle K. Hare[1]

Received 2 August 2011; revised 9 January 2012; accepted 14 January 2012; published 23 February 2012.

[1] Hyporheic flow can be extremely variable in space and time, and our understanding of complicated flow systems, such as exchange around small dams, has generally been limited to reach-averaged parameters or discrete point measurements. Emerging techniques are starting to fill the void between these disparate scales, increasing the utility of hyporheic research. When ambient diurnal temperature patterns are collected at high spatial resolution across vertical profiles in the streambed, the data can be applied to one-dimensional conduction-advection-dispersion models to quantitatively describe the vertical component of hyporheic flux at the same high spatial resolution. We have built on recent work by constructing custom fiber-optic distributed temperature sensors with 0.014 m spatial resolution that are robust enough to be installed by hand into the streambed, maintain high signal strength, and permit several sensors to be run in series off a single distributed temperature sensing unit. Data were collected continuously for 1 month above two beaver dams in a Wyoming stream to determine the spatial and temporal nature of vertical flux induced by the dams. Flux was organized by streambed morphology with strong, variable gradients with depth indicating a transition to horizontal flow across a spectrum of hyporheic flow paths. Several profiles showed contrasting temporal trends as discharge decreased by 45%. The high-resolution thermal sensors, combined with powerful analytical techniques, allowed a distributed quantitative description of the morphology-driven hyporheic system not previously possible.

Citation: Briggs, M. A., L. K. Lautz, J. M. McKenzie, R. P. Gordon, and D. K. Hare (2012), Using high-resolution distributed temperature sensing to quantify spatial and temporal variability in vertical hyporheic flux, *Water Resour. Res.*, *48*, W02527, doi:10.1029/2011WR011227.

1. Introduction

[2] There have been many studies of hyporheic exchange, from pore space to watershed scale, but it remains a challenge to quantitatively describe the structure and magnitude of hyporheic flow vectors at high resolution in the field. Conceptual diagrams of hyporheic flow paths through bed forms based on hydraulic head differentials are present throughout the literature, yet the magnitude of these flow vectors are generally either modeled or inferred from relatively sparse point measurements. *Harvey and Wagner* [2000] note that traditional point measurements were likely inadequate to describe the heterogeneous hyporheic zone in a useful way, so higher-resolution methods that move beyond the point scale are necessary. Hyporheic flux rates not only describe both the quantity of water moving from the stream into the subsurface, but also govern the residence time of hyporheic flow paths, which is a first-order control on the biogeochemical processing of dissolved nutrients [*Vroblesky and Chapelle*, 1994; *Zarnetske et al.*, 2011]. Because hyporheic flow occurs over a spectrum of flow vector magnitudes and residence times [*Ward et al.*, 2010], a spatially distributed method for measuring hyporheic exchange in situ must be flexible enough to yield accurate results under a wide range of flow conditions. Such a method would be especially useful in streams with complicated morphology and hyporheic exchange patterns, such as those affected by beaver impoundment [e.g., *Lautz et al.*, 2010].

[3] Recently there have been advances in the quantitative application of novel geophysical and analytical tools that move beyond point estimates of surface water seepage [*Cirpka et al.*, 2007; *Ward et al.*, 2010; *Pidlisecky and Knight*, 2012]. When temperature data is collected through time at high resolution within the streambed, the diurnal signal generated by colder nights and warmer days can be used to determine spatially distributed hyporheic flux dynamics. The diurnal, quasi-sinusoidal stream temperature signal propagates into the subsurface via conduction and advection. With increasing depth in the subsurface, the amplitude of the diurnal signal originating at the surface is attenuated and its phase is shifted forward in time. Disparities in the signal propagation from that predicted by pure conduction are

[1]Department of Earth Sciences, Syracuse University, Syracuse, New York, USA.
[2]Department of Earth and Planetary Sciences, McGill University, Montreal, Quebec, Canada.

0043-1397/12/2011WR011227

attributed to the advection of heat by hyporheic water [*Stallman*, 1965; *Constantz and Thomas*, 1996; *Anderson*, 2005; *Goto et al.*, 2005; *Hatch et al.*, 2006; *Keery et al.*, 2007]. Several studies have exploited differences in the diurnal signal between two depths in the vertical to estimate hyporheic flux using one-dimensional analytical heat transport models [*Hatch et al.*, 2006; *Keery et al.*, 2007; *Constantz*, 2008], and data for these models are commonly collected with discrete thermal loggers deployed in the field at relatively low spatial resolution [*Hatch et al.*, 2006; *Keery et al.*, 2007; *Lautz et al.*, 2010; *Rau et al.*, 2010; *Schmidt et al.*, 2011]. Although this application can provide valuable information regarding the average vertical flux condition between individual temperature sensors, spatial resolution is sacrificed, which can compromise the interpretation of complex oblique flow systems. Additionally, the ideal temperature sensor spacing varies with flux magnitude, which in turn may vary with both depth and time, so the ultimate temperature data set contains a high resolution of temperature observations in both dimensions to provide flexibility for 1-D modeling and analysis [*Hatch et al.*, 2006].

[4] Environmental applications of fiber-optic distributed temperature sensing (DTS) permit high-resolution, continuous temperature data collection through space and time in aquatic environments. DTS systems function by initiating a light pulse down an optical fiber and determining temperature along the fiber by measuring the ratio of temperature-independent Raman backscatter (Stokes) to temperature-dependent backscatter (anti-Stokes) of the light pulse [*Dakin et al.*, 1985; *Selker et al.*, 2006b; *Tyler et al.*, 2009]. The timing of these backscatter returns yields a measure of location, which for most systems can be resolved to approximately 0.25 to 1.0 m resolution over distances of several kilometers. Fiber-optic DTS has generally been applied to lotic systems to identify longitudinal temperature anomalies, which are used to locate and quantify groundwater discharge and hyporheic exchange [*Selker et al.*, 2006a; *Lowry et al.*, 2007; *Westhoff et al.*, 2007; *Moffett et al.*, 2008; *Briggs et al.*, 2011]. Modified DTS configurations include wrapping the fiber around a mandrel to increase spatial resolution dramatically [*Selker et al.*, 2006a; *Vogt et al.*, 2010; *Suárez et al.*, 2011]. These high-resolution sensors can be installed vertically in the streambed to capture the propagation of the diurnal signal with depth. The only previously published high-resolution DTS hyporheic application used one vertical profile and found that this method was especially useful for identifying heterogeneities in flux with depth [*Vogt et al.*, 2010].

[5] When stream velocities are reduced by beaver impoundment, their capacity to transport sediment is also significantly reduced; this results in large quantities of sediment being retained behind dams and the formation of complex bed forms [*Naiman et al.*, 1986], such as those known to enhance hyporheic exchange [*Harvey and Bencala*, 1993; *Kasahara and Wondzell*, 2003; *Gooseff et al.*, 2007]. Further, small dams drive water through the subsurface by creating punctuated head differentials along streams [*Lautz et al.*, 2006; *Hester and Doyle*, 2008]. Therefore beaver dams may generate a network of hyporheic flux "hot spots" governed by heterogeneity around individual dam complexes, enhancing microbial processing of dissolved nutrients.

[6] Our primary research interest for this study was to describe the complicated dynamics of vertical hyporheic flux in varied streambed morphology over time, while simultaneously introducing a powerful tool for investigating streambed fluxes. To do this research using ambient temperature, custom fiber-optic high-resolution temperature sensors (HRTS) were designed, constructed and deployed within the streambed. These specialized sensors were designed to minimize signal loss, allow in-series configuration, and be durable enough to permit installation by hand into the streambed. Data were collected continuously for 1 month along vertical streambed profiles upstream of two beaver dams in the western United States. We then applied a one-dimensional conduction-advection-dispersion model to the high-resolution diurnal temperature data to quantitatively estimate the vertical component of hyporheic flux. This allowed us to determine the penetration depth and structure of shallow hyporheic flow, which is likely most relevant to biogeochemical processing of stream carbon and nutrients, and to evaluate the viability and benefits of using multiple simultaneous fiber-optic HRTS over an extended period of time in the stream environment. The observed spatial patterns in flux determined with 1-D temperature modeling were supported with a conservative tracer injection. Additionally, as hyporheic exchange may be variable over summer flow recession as head gradients change, we investigated the temporal nature and correlation to potential forcing mechanisms of high-resolution vertical flux patterns.

2. Methods

2.1. Site Description

[7] Cherry Creek in Central Wyoming is a second-order stream that drains a 30 km^2 semiarid watershed on the east flank of the Wind River Range, and is managed by The Nature Conservancy of Wyoming [*Jin et al.*, 2009] (Figure 1). The creek supplies approximately half of the flow to Red Canyon Creek, a stream that has been extensively studied for surface water/groundwater interaction [*Lautz et al.*, 2006; *Lautz and Siegel*, 2006; *Fanelli and Lautz*, 2008; *Lautz et al.*, 2010]. After emerging from a narrow canyon, the lower 3 km of Cherry Creek flows along a relatively unconstrained valley floor with an approximately 1% grade and is lined mainly with glacial till and alluvial deposits of sand and gravel. The annual stream hydrograph is characterized by high spring flows during snowmelt and subsequent transition to base flow.

[8] During the summer of 2010 there were 13 beaver dams of varied size along the lower 1.3 km of Cherry Creek that had trapped large quantities of primarily fine sediments, generating large longitudinal steps in streambed morphology. The two dams specifically chosen for this study were located 75 m apart, approximately 1160 m upstream of the confluence with Red Canyon Creek (Figures 1 and 2). The larger dam, Dam 1, caused a 0.75 m drop in water surface elevation, while Dam 2 had a more modest 0.35 m drop at the beginning of the study period. Because of the high-flow conditions at the time of this study and recent flood damage and scouring around both dams, water did not stagnate upstream of the dams and had velocities comparable to other broad unimpounded sections

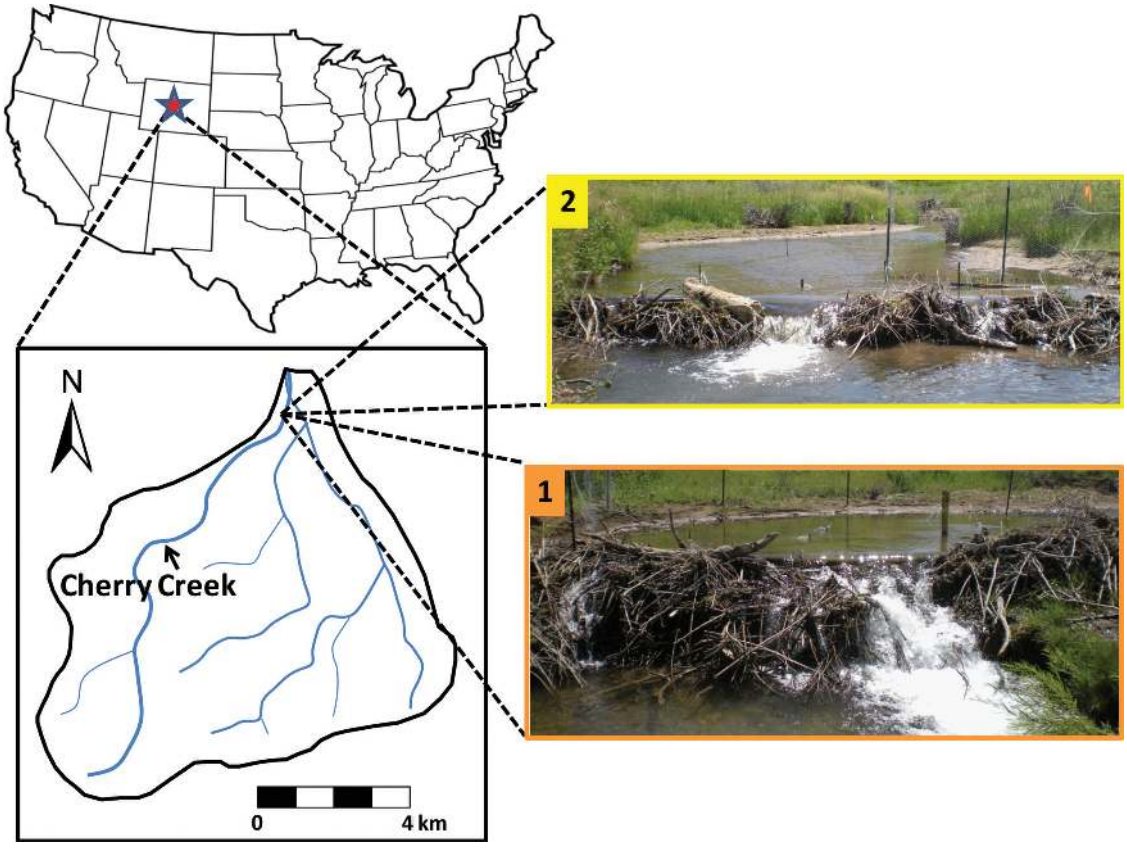

Figure 1. The Upper Red Canyon Creek drainage where Cherry Creek emerges from a deep, narrow canyon into the unconstrained valley floor along which many small beaver dams were located in the summer of 2010, including Dam 1 (0.75 m) and Dam 2 (0.35 m).

of the channel. The sediments surficial trapped behind both dams had a D_{50} of less than 2 mm, and consisted of fine gravel, sand, coarse clay and silt with abundant organic particles and the sediment-stream interface was not armored. The streambed morphology immediately above the two dams was similar, consisting of one dominant pool adjacent to a longitudinal bar structure. The bar at Dam 1 was located several meters upstream of the dam step (Figure 2a), while the bar at Dam 2 extended to the dam structure (Figure 2b).

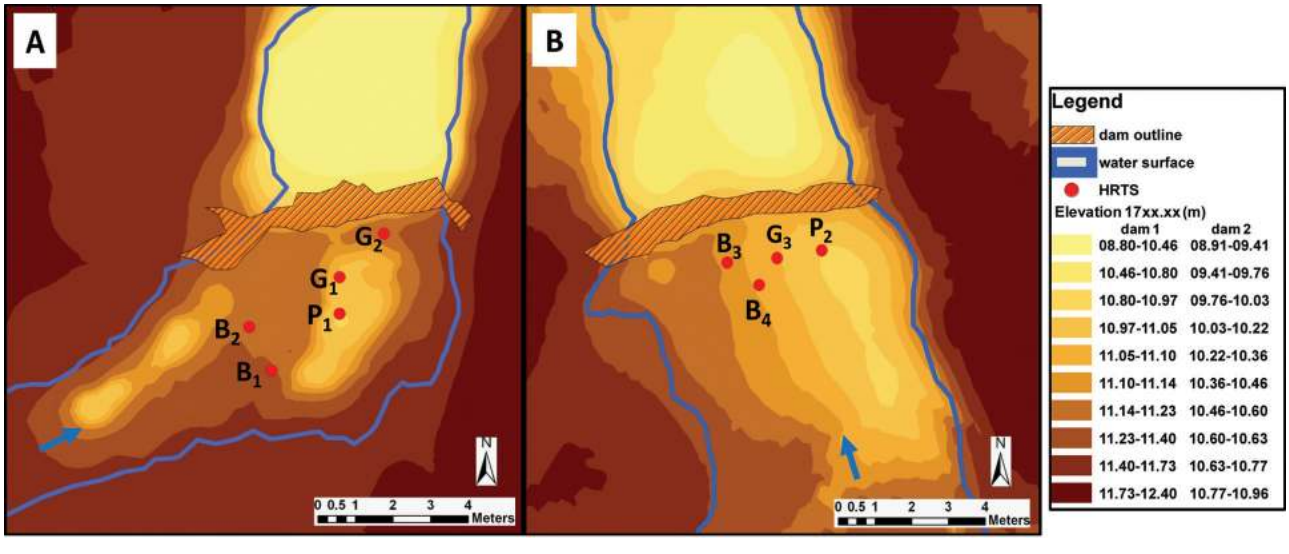

Figure 2. The streambed morphology around (a) Dam 1 and (B) Dam 2. The high-resolution temperature sensor (HRTS) locations were classified as bar (B), pool (P), or glide (G). The water surface profile reflects the conditions on 14 July 2010 near the beginning of the study period.

2.2. Reach Hydrologic, Geomorphic, and Climatic Characterization

[9] Stream discharge and mean velocity were measured daily over the study period at the reach outlet with a top setting wading rod equipped with a handheld acoustic Doppler velocimeter (SonTek/YSI FlowTracker ADV) that had a velocity range of 0.001–4.0 m s^{-1}. The channel was modified to a rectangular shape and cleared of large cobbles to provide optimal conditions for velocity-area measurements, and each velocity measurement was integrated for 40 s. Stream stage was monitored at lower temporal resolution above each dam by measuring changes in water surface elevation relative to a known datum. Sediment core collection was attempted at the time of HRTS installation but core integrity was poor and this data was not used. A spatial survey of the dams, banks, streambed morphology and HRTS locations was collected using a Nikon Nivo 5.M total station. At the research site, high temporal resolution stream and air temperature were recorded using loops of the in-line fiber-optic cable located within the water column or on the shaded bank, respectively. Groundwater was periodically monitored for temperature in riparian piezometers adjacent to each dam, which were screened between 0.75 and 1.0 m below the land surface, and at deeper downstream water table wells located outside of the riparian zone.

2.3. High-Resolution Temperature Sensing

[10] To investigate spatial patterns in vertical hyporheic flux, custom fiber-optic HRTS were constructed and installed within the subsurface upstream of two dams to determine the vertical component of hyporheic seepage flux. The DTS unit used for this application (Agilent Distributed Temperature Sensor N4386A) had a minimum spatial resolution of 1 m along optical fiber. Bend-insensitive fiber-optic cable was wrapped around a standard 4.8 cm PVC core, 1 m in length, to create a HRTS with 0.014 m vertical resolution. The fiber-optic cable used for this application, Corning ClearCurve^{TM}, is designed to minimize light loss in wrapped configurations and had never been used for environmental DTS before. Our laboratory tests indicated signal loss along the wrapped fiber was only slightly higher than for unwrapped fibers ($\sim$1.4 dB km^{-1}) and the strength of signal transmission permitted several HRTS to be run in series in dual ended mode. The ClearCurve fibers were packed in hydrophobic gel and installed within a 1.65 mm diameter stainless steel tube by AFL Telecommunications. These cables were wrapped tightly by hand around each PVC core, which was prethreaded at a specific pitch to allow a consistent wrap of the fiber-optic cable without physical contact between consecutive coils, and yield the desired 0.014 m vertical spatial resolution. The steel tube protected the fragile glass fiber and allowed for a physically robust design that could be installed within the compacted streambed sediments. The threaded PVC rods were wrapped from top to bottom and the fiber was brought back to the top along the outside of each HRTS. At least 15 m of fiber were left at the top of the rod to facilitate connection to the next HRTS in series (Figure 3).

[11] A total of nine HRTS were installed vertically within the streambed sediments to at least 0.75 m depth,

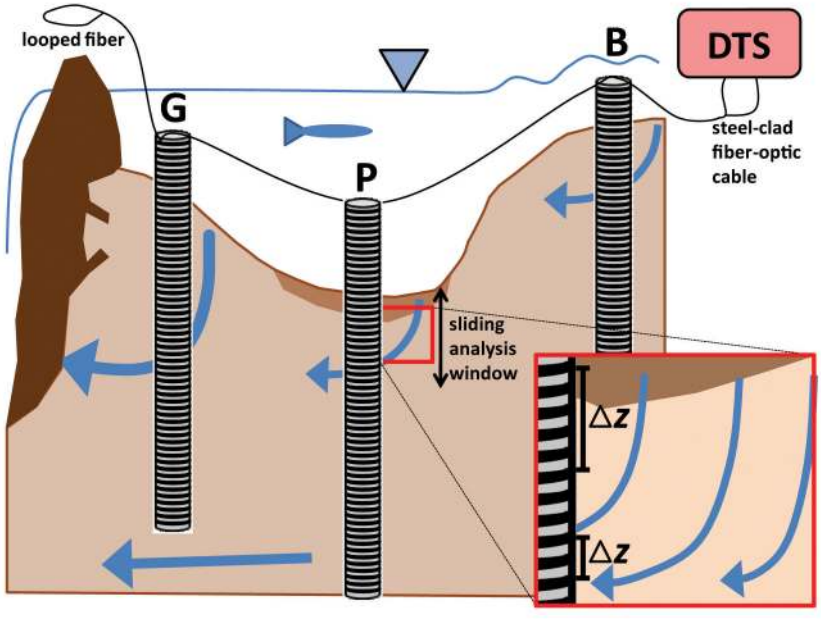

Figure 3. A longitudinal cross-section view of a bar-pool-dam sequence and the wrapped configuration of the HRTS, which provided 0.014 m spatial temperature resolution in the vertical. Two fibers ran through the stainless-steel housing and were connected through several HRTS in series, the end of which was spliced and looped to allow bidirectional laser pulses from the distributed temperature sensor (DTS) to improve calibration. The rods were installed in streambed bars (B), pools (P), and glides (G), and the inset shows how they were found to cut across a spectrum of oblique hyporheic flow paths that transitioned from vertical to horizontal with depth, patterns that were described using the integrated sliding analysis windows. The optimal window size (Δz) decreases with vertical flux magnitude.

five upstream of Dam 1 (B_1, B_2, P_1, G_1, G_2) (Figure 2a) and four upstream of Dam 2 (B_3, B_4, P_2, G_3) (Figure 2b). Installation locations were chosen to best reflect the observed heterogeneities in streambed morphology, which as discussed above consisted of one dominant pool and bar above each dam, so the naming scheme has been reduced to: B = bar, P = pool and G = glide locations. The HRTS were also installed at varied distance upstream from the dam structure (Figure 2 and Table 1). Specifically G_2, B_3, G_3 and P_2 were all installed 1 m upstream from their respective dams to control for longitudinal elevation head change and isolate the effects of morphology and associated disparities in streambed hydraulic conductivity. To facilitate installation, a steel pipe with drive point of similar size to the HRTS was driven by sledge into the bed and withdrawn to create a guide hole. The HRTS were then immediately inserted into the hole and pounded gently into the sediments to the desired depth. They were connected in series using a Fujikura FSM-18S Fusion Splicer to create one continuous length of fiber that ran out and back through all of the HRTS consecutively, and was attached at each end to respective channels of the Agilent DTS unit (Figure 3).

[12] The advantage of this looped configuration was to allow the instrument to operate in "double-ended" mode, in which bidirectional laser pulses along the fiber greatly simplify the calibration processes. Calibration is necessary because of the inherent attenuation of the laser pulse as it travels down the optical fiber and passes through spliced connections [*Tyler et al.*, 2009]. By running the Agilent Sensing DTS unit in double-ended mode, signals generated in both directions were integrated, and the optical fiber properties were determined over the measurement by the onboard DTS software. The instrument was programmed to update temperature traces at 1.0 m increments every 10 s on alternating channels which were integrated at 10 min time intervals by the DTS software to yield a single temperature estimate every 20 min for each location along the HRTS array. The DTS system was used to collected temperature measurements from 13 June to 10 August.

[13] The precision of the DTS system in this specific configuration was 0.2°C (standard deviation) according to software provided by the instrument manufacturer. The accuracy of a DTS system is dependent on calibration at known points, and it was necessary to perform this calibration continuously over time because of variable instrument drift which can change the offset between the measured and true temperatures. The system was kept thermally calibrated using an ambient temperature water bath, which was mixed by a 950+ L h^{-1} bilge pump run continuously over the period of data collection. Following the recommendation of *Tyler et al.* [2009], 40 m of cable was coiled through the bath and three Thermochron iButton temperature sensors with 0.5°C accuracy and 0.0625°C precision were used to independently monitor bath temperature. We selected a subset of iButtons that most closely measured the central temperature distribution of a batch of 80 and compared well to a high-precision thermistor, although for this application, where we compare temperature records at varied depth, absolute accuracy is much less important than data precision. During data postprocessing, the entire data set was adjusted for offset between the 40 m reference coil and the mean of the independent iButton records. Spatial calibration of the DTS fiber was accomplished by applying distinct temperature signals to the cable at known reference points. The sediment-stream interface was identified for each temperature profile and periodically monitored for possible changes on the basis of scour and deposition using a waterproof chemical heat source. No significant change in this datum was observed over the period of data collection. During data postprocessing, the temperature record for each individual HRTS was isolated and scaled to the true vertical distance using the known scale factor of 1.0 m to 0.014 m.

Table 1. Morphology and Longitudinal High-Resolution Temperature Sensor (HRTS) Distances Above Beaver Dams 1 and 2

HRTS	Distance From Beaver Dam (m)	Morphology at HRTS Location
B_1	4.3	edge of bar, fine gravel/silt
B_2	3.1	middle of bar, fine gravel/silt
B_3	1.0	middle of bar, fine gravel/silt
B_4	1.7	middle of bar, fine gravel/silt
P_1	2.7	bottom of pool, fine silt/clay/organics
P_2	1.0	bottom of pool, fine silt/clay/organics
G_1	1.7	midglide, fine silt/sand
G_2	1.0	end of glide, silt/sand/gravel
G_3	1.0	midglide (lateral), fine gravel/silt/sand

2.4. High-Resolution Vertical Flux Determination

[14] Once the calibrated temperature records for each HRTS were identified and scaled, vertical flux estimates were made at high spatial and temporal resolution using changes in the diurnal temperature signal with depth along each HRTS profile. *Hatch et al.* [2006] and *Keery et al.* [2007] presented two similar methods to calculate vertical water flux on the basis of the one-dimensional conduction-advection-dispersion equation of *Stallman* [1965]:

$$\frac{\partial T}{\partial t} = k_e \frac{\partial^2 T}{\partial z^2} - q \frac{C_w}{C} \frac{\partial T}{\partial z}, \tag{1}$$

where T is temperature (°C), t is time (s), k_e is the effective thermal diffusivity of the saturated sediment ($m^2\ s^{-1}$), z is depth (m), C_w is the volumetric heat capacity of the water, C is the volumetric heat capacity of the saturated sediment ($J\ m^{-3}\ °C^{-1}$) (a volume weighted average derived from C_w, porosity (n), and C_s, the volumetric heat capacity of sediment), and q is fluid flux ($m\ s^{-1}$), for which a positive value indicates downward flow. This equation is solved analytically using the *Hatch et al.* [2006] amplitude method as

$$q = \frac{C}{C_w}\left(\frac{2\kappa_e}{\Delta z}\ln A_r + \sqrt{\frac{\alpha + v^2}{2}}\right), \tag{2}$$

where A_r is the ratio of amplitudes between a lower and an upper temperature signal (unitless), Δz is the vertical distance between the lower and an upper temperature signal in the streambed (m), v is the velocity of the thermal front ($m\ s^{-1}$) and κ_e ($m^2\ d^{-1}$) is the effective thermal diffusivity defined as

$$\mathcal{K}_e = \left(\frac{\lambda_o}{C}\right) + \beta|v_f|, \tag{3}$$

where λ_o is the baseline thermal conductivity of the saturated sediment (J s^{-1} m^{-1} °C^{-1}), β is thermal dispersivity (m), and v_f is the linear particle velocity (m s^{-1}); finally, α is determined by

$$\alpha = \sqrt{v^4 + \left(\frac{8\pi\kappa_e}{p}\right)^2}. \quad (4)$$

[15] Because the Hatch model is predicated on a sinusoidal temperature signal with a period of 24 h, it is desirable to filter nonideal field temperature records to better isolate the sinusoidal diurnal signal, which can be complicated by both local environmental factors and intrinsic system noise [*Hatch et al.*, 2006; *Keery et al.*, 2007; *Vogt et al.*, 2010]. This is particularly apparent when using the DTS in this configuration, as the relatively low HRTS precision (0.2°C) introduces noise that can complicate analysis of the nonstationary amplitude and phase information of the diurnal signal. We used the new MATLAB program VFLUX [*Gordon et al.*, 2012] as an integrated way to both extract the 24 h signal from the data and calculate flux at high temporal and spatial resolution. Specifically VFLUX was used (1) to low-pass filter the raw temperature record, (2) to isolate the diurnal component of the temperature signal using dynamic harmonic regression (DHR) and extract its amplitude (one half the maximum minus the minimum of the wave) and phase information, (3) to calculate flux every 2 h at a range of depths using multiple "sliding analysis windows" to detect changing flux magnitude with depth, and (4) to use the Monte Carlo method to incorporate uncertainty in streambed thermal parameters to assess potential for error of fluxes around zero m s^{-1}.

[16] First, the original sampling rate of 20 min was reduced to 2 h through an antialiasing decimation technique that preserved the diurnal signal information gained by using the original 20 min sampling rate. This low-pass filtering removed any components of the temperature record with a period of less than 4 h, effectively eliminating much of the high-frequency noise introduced by the low HRTS precision and short-term weather fluctuations. DHR is a method of nonstationary time series signal processing that is used to extract periodic signal(s) of interest [*Young et al.*, 1999], and VFLUX runs the MATLAB Captain Toolbox program [*Young et al.*, 2010] to perform the DHR analysis. The Captain Toolbox DHR software has also been used by previous researchers [*Keery et al.*, 2007; *Vogt et al.*, 2010], and *Keery et al.* [2007] specifically notes that the extracted 24 h temperature signal is not an approximation or smoothed copy, but a real component of the measured temperature series.

[17] Subsequently, 2 days of the diurnal signal were removed from each end of the temperature record to remove possible adverse edge effects of the filtering process [*Keery et al.*, 2007]. VFLUX was then used to determine vertical hyporheic flux at a range of depths through the difference in diurnal signal amplitude between any measured depth and a location deeper in the bed along the same vertical profile of temperature (equation 2). These two temperature records bound a "window," or distance over which the vertical component of flux is determined (Figure 3). VFLUX uses the phase information generated from the DHR program to align analogous points in the temperature signals at each edge of the window (upper and lower) and calculate a flux for every 2 h time step using the amplitude ratio between the two signals [*Gordon et al.*, 2012].

[18] Because any point estimate of vertical flux is essentially an integration of the vertical component over the length of the window, we interpret each flux estimate as representative of the midpoint between the two depths. The window size is held constant, and incrementally shifted down the vertical profile as flux is calculated at the same spatial resolution as the original data set (0.014 m) at every time step. Therefore the sliding analysis window is used to create a high-resolution map of vertical flux along the HRTS profile. It should be noted that although window size may vary, the spatial resolution of the resultant vertical flux profile is determined by the HRTS spatial resolution (0.014 m), and is therefore constant for all windows.

[19] It was desirable to use the smallest window possible between temperature observations to distinctly identify abrupt changes in flux with depth which would be blurred when averaging over too large an interval. Additionally, a smaller window between temperature observations allows more flux information to be preserved very close to the streambed boundary, where we can expect flow to be truly vertical and which can be used to estimate total flux into the streambed. Although a small sliding analysis window is desirable for optimizing spatial resolution, higher flux rates must be resolved using a relatively large window, so that a decrease in amplitude can be adequately detected (e.g., window large enough to generate an $A_r < 1$). Therefore the optimal (minimal) size sliding analysis window increases with vertical flux magnitude (as illustrated in the inset in Figure 3). Because we may expect the patterns of shallow hyporheic flux to vary both with stream morphology and depth, multiple window sizes are necessary to optimize our interpretation of complicated flow systems. To address this need, we used six consecutively sized analysis window sizes along each HRTS profile at increments of 0.014 m. For example, window sizes of 0.069, 0.083, 0.097, 0.110, 0.124, and 0.138 m were used for the HRTS G_2 analysis. We then generated a composite flux matrix from those six sliding analysis windows by averaging flux estimates at analogous depths between the vertical profiles determined using each window size. This maximized results in high-flux zones, while still being able to resolve transitions to low flux at depth with high spatial resolution. The optimal six window range was determined through trial and error for each HRTS, as that which generated the most complete composite matrix with the fewest number of incalculable values of flux through time and space (e.g., windows for which A_r is 1 or greater) yet preserve information close to the sediment/water interface.

[20] It was advantageous to perform these flux calculations automatically using VFLUX, as six windows integrated over our HRTS lengths and temporal period resulted in over 100,000 individual 2 h flux calculations per profile. Additionally, the peak amplitude information generated during the DHR procedure was used to determine the depth at which the mean amplitude of the diurnal signal was less than the 0.2°C precision of the DTS system, which is the

point at which the signal cannot be distinguished from noise [*Vogt et al.*, 2010]. This provided an objective measure of the depth at which to stop calculating flux because of a lack of signal, and this extinction depth varied significantly with the magnitude of downward flux observed at each HRTS location. Streambed thermal parameter inputs to the model and their uncertainty range (Table 2) were estimated through field observation and the relationships presented by *Lapham* [1989], and are consistent with the range of previous investigations of downstream reaches in the same drainage [*Fanelli and Lautz*, 2008; *Lautz et al.*, 2010]. Monte Carlo analysis was performed using the VFLUX software, which randomly varied all thermal parameters simultaneously within a standard normal distribution defined by the corresponding estimated parameter uncertainty (Gordon et al., submitted manuscript, 2011) (Table 2). The results from 500 realizations were integrated to determine 95% confidence intervals around flux values that ranged from positive to negative through time at the 0.15 m HRTS B_3 location using a 0.07 m analysis window. This allowed the estimation of bounds for determining whether flux was significantly different than 0 m s^{-1} under these site-specific conditions.

[21] Vertical flux rates determined with heat tracing were compared to nominal travel times [*Triska et al.*, 1989; *Harvey et al.*, 2005] estimated during a 9 h constant rate Cl^- injection on 8–9 August. Profiles of pore water were collected in the streambed three times (3.7, 5.3, and 8.3 h into the injection) within 0.2 m of each HRTS using piezometer nests screened at 0.05–0.10, 0.15–0.20 and 0.30–0.35 m depth intervals. Nominal vertical velocities were multiplied by the general porosity determined for the site (0.35), which was assumed to equal effective porosity, to calculate vertical hyporheic flux which is directly comparable to that derived from the temperature records.

2.5. Temporal Evaluation of Flux Patterns

[22] A linear trend analysis was performed for every depth along each HRTS profile to identify any general patterns in flux through time. Hyporheic flux patterns may be expected to change as the streambed pressure head boundary changes through time because of changing stream discharge and associated velocity and stage. Therefore, changes in vertical hyporheic flux over time were compared to changes in stream discharge over time, as a proxy for total pressure head change. The strength and significance of correlation between discharge and vertical flux were explored for every depth along each HRTS profile.

Table 2. Estimated Thermal Properties of the Saturated Streambed Used for l-D Modeling of Vertical Hyporheic Flux[a]

Thermal Parameter	Estimated Value
Porosity n	0.35 (0.05)
Volumetric heat capacity of the sediment C_s	2.09×10^6 (8.4×10^4) J m^{-3} °C^{-1}
Volumetric heat capacity of the water C_w	4.18×10^6 (1.3×10^4) J m^{-3} °C^{-1}
Thermal dispersivity β	0.001 (0.0001) m
Thermal conductivity of the saturated sediment λ_o	1.4 (0.21) J s^{-1} m^{-1} °C^{-1}

[a]The estimated uncertainty (standard deviation) of each parameter used for the Monte Carlo analysis is given in parentheses.

3. Results

3.1. Reach Hydrologic and Climatic Characterization

[23] Over the period of HRTS data collection (13 July to 10 August 2010) streamflow at the outlet of Cherry Creek dropped by 45%, from 383.4 to 210.7 L s^{-1} (Figure 4). This corresponded to a generally steady drop in mean stream velocity at the outlet from 0.72 m s^{-1} to 0.55 m s^{-1}, while stage decreased by approximately 10% above both dams 1 and 2. The ambient air temperature showed no significant trend over the month but fluctuated between 5.4°C and 36.3°C, with notably warmer and colder stretches (Figure 4). These short-duration temperature changes were strongly dampened in the stream where temperature varied only between 10.0°C and 17.7°C because of relatively high flow conditions and velocities which maintained the cold base flow/snowmelt signal after the stream emerged from a deep, shaded canyon 2 km upstream. The diurnal signal in the stream, which is the input signal to the streambed, had a small amplitude that varied between 0.6°C and 1.9°C with ambient weather conditions (Figure 4). Repeat differential gauging at the head (264.6 L s^{-1}) and tail (256.6 L s^{-1}) of a 650 m reach encompassing both dams on 29 July yielded mean values that varied less than 3% over the reach, or the mean error estimated with the FlowTracker instrument (SonTek/YSI FlowTracker ADV).

3.2. High-Resolution Temperature Sensing

[24] For all HRTS, the diurnal signal was evident at shallow depths and was most pronounced during the continuous period of warm weather from approximately 27 July to 2 August. Additionally, there was a time lag (or phase shift) and reduction in amplitude of the diurnal signal with depth; these effects varied strongly by location, indicating varied magnitudes of heat transport into the subsurface (Figures 5a and 6). The nearly vertical patterns of amplitude with depth depicted in Figure 6 for the G_1, G_2, G_3 and B_4 locations indicate conservative transport of the diurnal signal

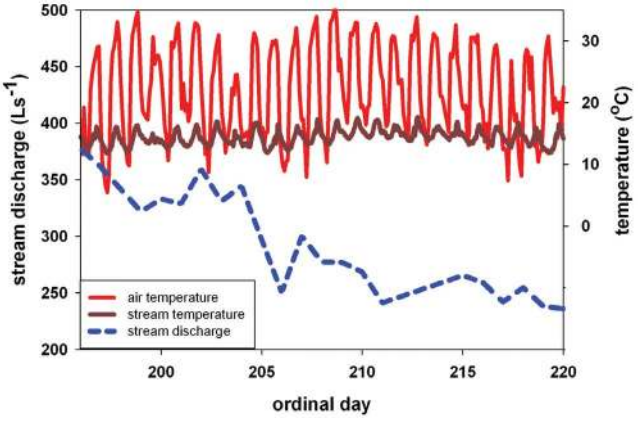

Figure 4. Daily discharge and both air and stream temperatures at Cherry Creek over the period of record. The ambient air and stream temperatures had no consistent trend over the period, and the stream strongly muted the ambient air temperature and diurnal oscillations.

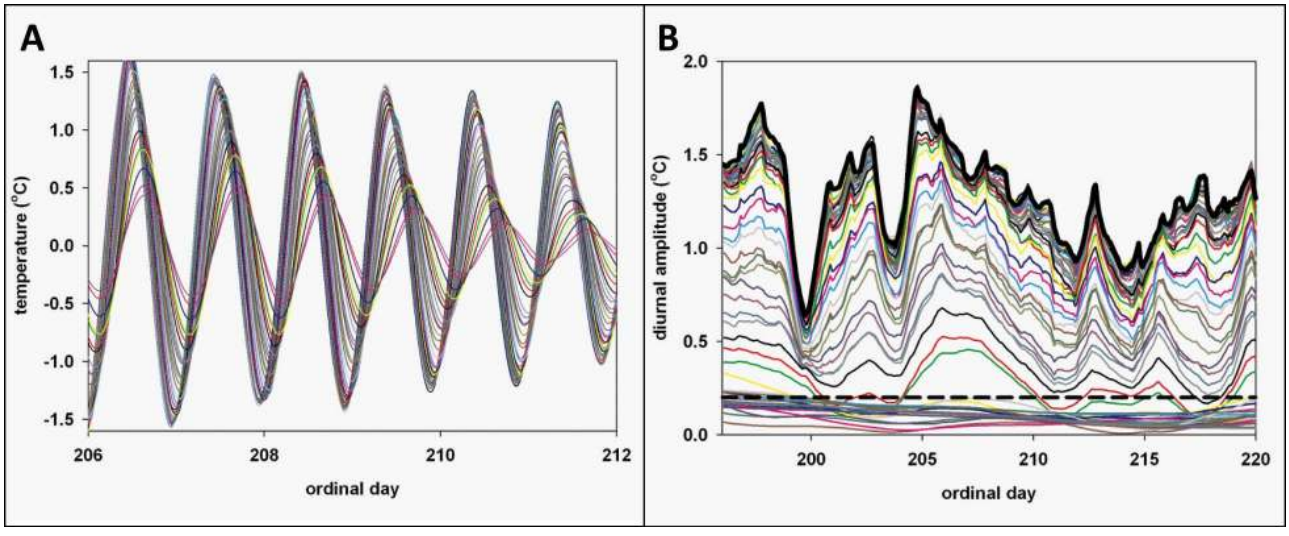

Figure 5. (a) The extracted diurnal signals over several days in late July 2010 for all depths that had signal amplitude greater than HRTS precision (0.2°C) along the G_2 profile. Increasing depth into the streambed was characterized by the reduction of signal amplitude and phase shift forward in time. (b) The changes in the amplitude of the stream diurnal signal (thick black line) through time and subsequent reduction with propagation into the streambed along G_2 until the HRTS precision was reached (dashed line).

(high flux). Temperature was plotted by depth through time along each profile to explore patterns in the propagation of heat (Figure 7). Similar patterns of thermal transport were observed within analogous morphological units, with the most variability among the four HRTS installed within bars. The bar profiles farthest from the dam, B_1 and B_2, had the shallowest propagation of the diurnal signal, while profiles B_3 and B_4, located closer to their respective dams, showed a more pronounced propagation of the diurnal signal (Figures 6 and 7 and Table 3) and greater transport of heat to depth.

[25] The temperature patterns for the two HRTS installed within the bottoms of pools, P_1 and P_2, were very similar, having the coldest temperatures at depth of any of the HRTS locations (Figures 6 and 7). Temperatures from deeper than 0.7 m ranged between 10.0°C and 12.0°C over the first half of the month, which was comparable to the temperature of groundwater sampled in the deep hillslope water table wells (10.6°C–12.6°C), but lower than the temperature of adjacent riparian wells (approximately 14.0°C). The HRTS located along glides close to the dams, G_1, G_2, and G_3, had consistently strong penetration of the diurnal signal, as indicated by the vertical banding of the temperature signal with little apparent phase shift shallower than the 0.2 m depth (Figure 7). As with the B_3 and B_4 bar locations, there was notable propagation of heat to the deepest locations of HRTS profiles (greater than 0.7 m), although the diurnal signal was generally indistinguishable there because of attenuation below the HRTS precision.

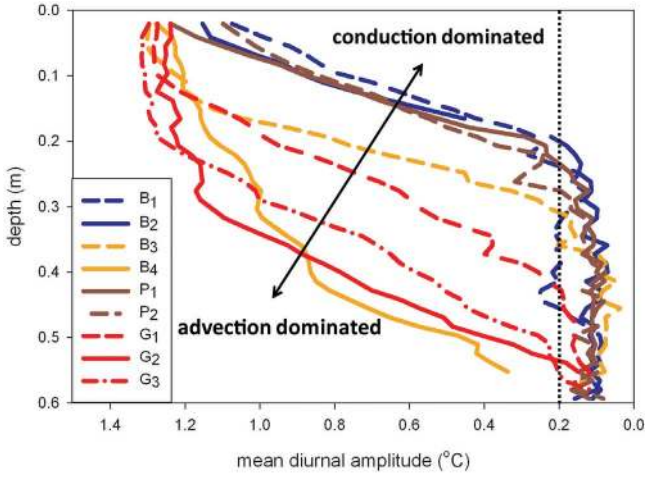

Figure 6. The variable attenuation of the diurnal signal with propagation into the streambed along each HRTS profile. The sensor precision is marked by the vertical dotted line.

3.3. High-Resolution Vertical Flux

[26] Attenuation of the diurnal signal amplitude to less than 0.2°C was used to determine the depth to which the true diurnal oscillation of temperature could be distinguished from measurement noise and therefore the maximum depth at which flux could be reasonably determined. This depth varied greatly by HRTS location but was greatest at the glides and location B_4 (Table 3). Sliding analysis windows of optimal size for the 1-D model were applied to the data from each HRTS, as described in Methods, and results using those analysis windows were integrated to produce quantitative vertical flux matrices by depth through time (Table 3 and Figure 8). The flux profiles had distinct boundary transitions from positive (downward) flux near the streambed interface to no positive vertical component at specific depths, though this depth varied strongly by morphologic unit. The median flux value at each depth was determined over the entire period of record to facilitate inter-HRTS comparison and more clearly depict spatial patterns (Figure 9).

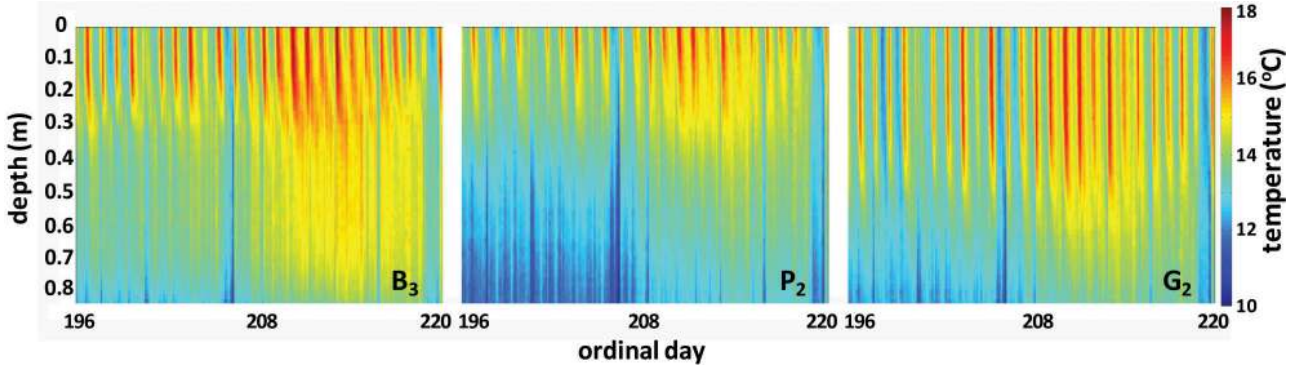

Figure 7. The temperature records at 0.014 m spatial and 2 h temporal resolution for representative bar (B_3), pool (P_2), and the glide (G_2) profiles. Each "pulse" of hot color indicates the propagation of the warm daytime signal from the sediment-water interface into the streambed.

[27] Similar to the patterns of amplitude with depth described in section 3.2 (Figure 6), patterns of vertical flux with depth at the bar locations were the most heterogeneous of the morphologic units. At the two most upstream bar locations (B_1 and B_2) vertical flux was modest at the bed interface (less than 0.4 m d^{-1}) and both had a very shallow penetration depth of 0.12 m, above which vertical flux had a positive vertical component (Table 3 and Figures 8 and 9). These patterns also showed a transition to negative flux below the 0.12 m depth, at which the diurnal signal was still relatively strong (greater than 0.5°C). The other bar locations, B_3 and B_4, were located closer to their respective dam step and had much higher vertical flux at the bed interface (approximately 0.9 m d^{-1}), although flux at B_3 was again very shallow and had no detectable vertical component below 0.18 m. In contrast, the vertical flux at B_4 was strong (greater than 0.7 m d^{-1}) above 0.35 m, and below it transitioned to no vertical flow at a depth of 0.5 m, which was the deepest penetration of downward flux along any profile. The temporal flux patterns at B_4 were the most variable, and no flux could be determine for several discrete time periods and depths because of amplitude ratios above 1.0.

[28] The flux patterns observed at the pool locations (P_1 and P_2) were very similar, although P_2 was much closer to the respective dam step (1.0 versus 2.7 m) (Figures 2, 8, and 9). Vertical flux was determined to a depth of 0.16 m in both locations, and produced negative values by 0.12 m (Table 3). Flux at the bed interface at P_2 was slightly greater than at P_1 (0.4 versus 0.3 m d^{-1}, respectively), although these values were quite modest and similar to those observed at the two upstream bar locations. Both profiles showed a change to negative flux with depth, and this effect was most noticeable at P_1. The depth of transition to negative flux varied by approximately 0.05 m and showed similar temporal patterns between profiles.

[29] The glide locations (G_1, G_2, and G_3) had consistently strong vertical flux which extended deep into the subsurface (Table 3 and Figures 8 and 9). At the streambed interface of G_1 vertical flux was 1.3 m d^{-1} and attenuated quickly at shallow depths, then in a slow linear fashion until there was no vertical component by 0.34 m. G_2 was located in the same glide, 0.7 m downstream of G_1, and 1.0 m from the dam step (Figure 2a). The shallowest median vertical flux at this location was 1.6 m d^{-1}, which was the largest value determined for any HRTS. Flux could not be estimated for the zone 0.0 to 0.06 m below the sediment water interface because amplitude ratios were so high that the largest HRTS spacings (0.097–0.166 m) of any profile had to be used. The vertical flux component was greater than 1.5 m d^{-1} above 0.12 m, then dropped off rapidly before leveling off and dropping off again until being extinguished at 0.45 m (Figures 5, 8, and 9). G_3 was located at the glide of the downstream dam, also 1.0 m back from the respective dam. Initial vertical flux here was greater than 1.4 m d^{-1} above 0.08 m, below which it quickly fell off to 0.6 m d^{-1} and reduced at a slower rate until reaching 0 m d^{-1} at 0.41 m.

[30] The Monte Carlo uncertainty analysis based on a plausible range of streambed thermal parameters (Table 2) indicated that flux estimates were most precise at approximately 0.4 m d^{-1}, while uncertainty increased as flux transitioned to negative through time at the 0.15 m B_3 location (Figure 10). The 95% confidence interval was used to determine when flux estimates may be considered significantly different from zero m d^{-1} under these system-specific conditions. This range was found to be ±0.1 m d^{-1}, and these bounds were applied to the median flux estimates as a guide for flux pattern interpretation (Figures 9 and 10).

[31] Hyporheic pore water was collected three times during a 9 h constant rate Cl^- injection on 8–9 August to estimate flux rates and hyporheic connectivity in support of the 1-D vertical flux modeling. All sampling locations and

Table 3. Optimized Sliding Analysis Window Range and Vertical Flux Calculation Depth Along Each Profile

HRTS	Range of Six Analysis Window Spacings, Every 0.014 (m)	Maximum Depth at Which Flux Could Be Resolved (m)	Depth of Transition to No Positive Vertical Flux (m)
B_1	0.014–0.083	0.17	0.12
B_2	0.014–0.083	0.16	0.12
B_3	0.055–0.124	0.28	0.18
B_4	0.083–0.152	0.57	0.50
P_1	0.014–0.083	0.21	0.13
P_2	0.014–0.083	0.20	0.14
G_1	0.069–0.138	0.41	0.34
G_2	0.097–0.166	0.52	0.45
G_3	0.083–0.152	0.50	0.41

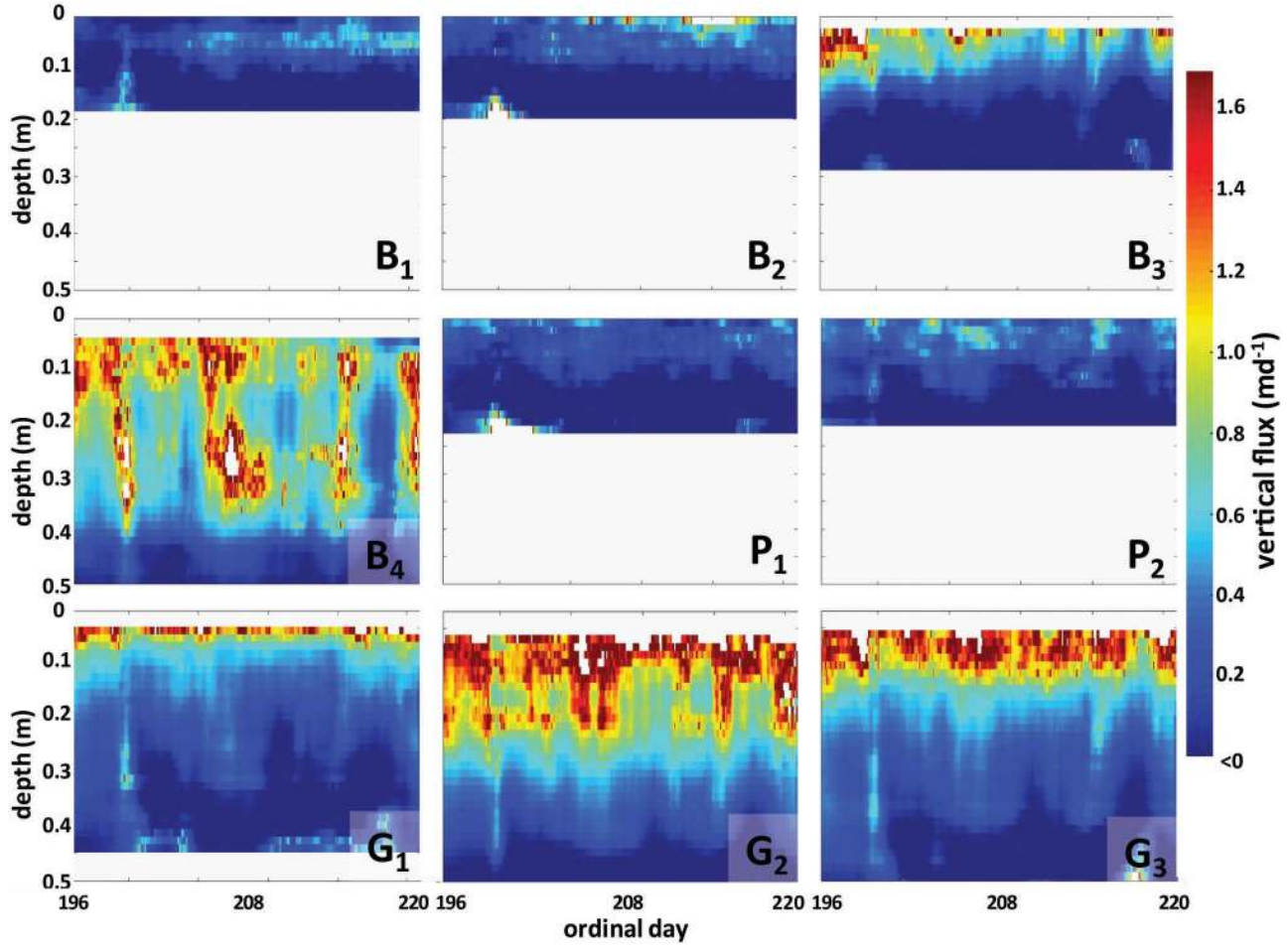

Figure 8. Vertical flux through time along each profile to the 0.5 m depth, with notable similarities by the general streambed morphology classification: B (bar), P (pool), and G (glide). The white area on the graphs indicates the depths at which the vertical component of flux could not be resolved because of minimal diurnal signal propagation.

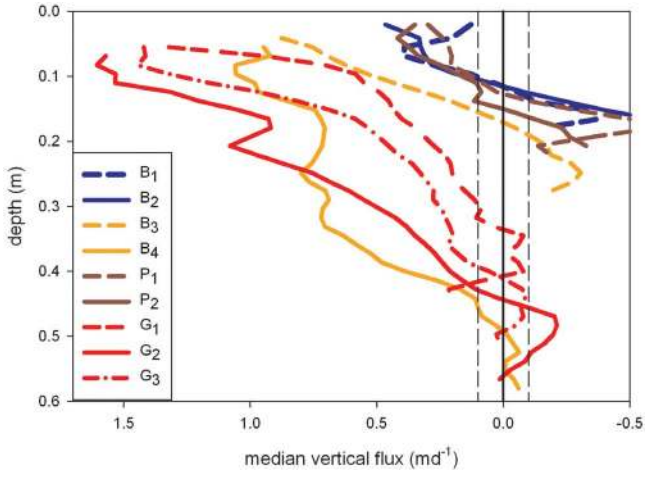

Figure 9. The median vertical flux for the study period with depth for each HRTS profile; the dashed lines show the region flux that may not be considered significantly different than zero (± 0.1 m d^{-1}) on the basis of a reasonable range of thermal parameter uncertainty.

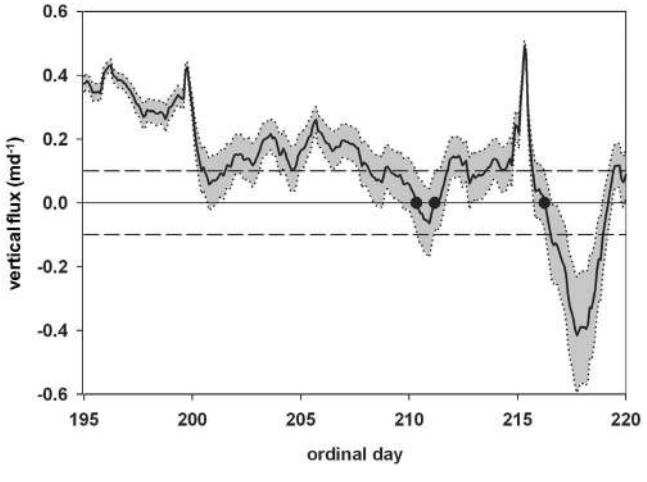

Figure 10. The 95% confidence interval around flux through time at the 0.15 m depth along HRTS B_3. The locations where flux was zero (circles) were used to determine the ± 0.1 m d^{-1} where flux estimates could not be considered significantly different from zero (dashed lines) on the basis of thermal parameter uncertainty.

depths had elevated levels of Cl^- 8.3 h into the injection, indicating all locations were connected to the stream. Locations G_2, G_3 and B_4 were composed of over 80% stream water at 0.3 m depth by the end of the tracer injection. These locations corresponded to the highest modeled vertical flux rates of greater or equal to 0.69 m d^{-1}. Locations composed of less than 50% stream water at a shallower depth of 0.15 m at the end of the tracer injection corresponded to locations with modeled vertical flux rates of less than 0.4 m d^{-1}. In general the Cl^{-1} tracer arrival times were inversely correlated with flux rates determined with the 1-D model, but there was some significant variability especially along the bar profiles.

3.4. Temporal Evaluation of Flux Patterns

[32] The linear trend analysis revealed that B_1 and B_2 had increasing flux through time while B_3 and B_4 had decreasing flux at shallow depths. Correlations between flux at every depth and stream discharge, with $p \leq 0.01$, were plotted by depth for each HRTS, and several consistent patterns were evident (Figure 11). As expressed in the linear trends, the two most upstream bar locations had similar, strong negative correlations with discharge (more negative than −0.5) within the upper 0.1 m of the bed, indicating increased seepage as flow decreased. There was a brief transition to weaker positive correlation at depth corresponding to the change to negative flux. The downstream bar locations had generally strong (B_3) or moderate (B_4) positive correlations to discharge over the upper 0.2 m, indicating different mechanisms controlling flux between the upstream and downstream bar locations (Figures 11, 12). Correlations at the pool locations were variable; P_1 had the only other consistently negative correlation to discharge (apart from the upstream bars) within the upper 0.1 m, and the downstream P_2 had little correlation in this range. At depth, both pool locations showed moderate, positive correlations between flux and discharge, at the same depth as the transition to negative flux. Finally, glide locations G_1 and G_3 had positive correlation between flux and discharge at most depths, while G_2 had positive correlation over only a narrow range of depths. In summary, where amplitudes were relatively high and flux estimates more reliable, most locations showed positive correlation to discharge. The exception was the most upstream bar and pool locations (B_1, B_2, P_1), which had a consistently strong negative correlation to discharge at shallow depths.

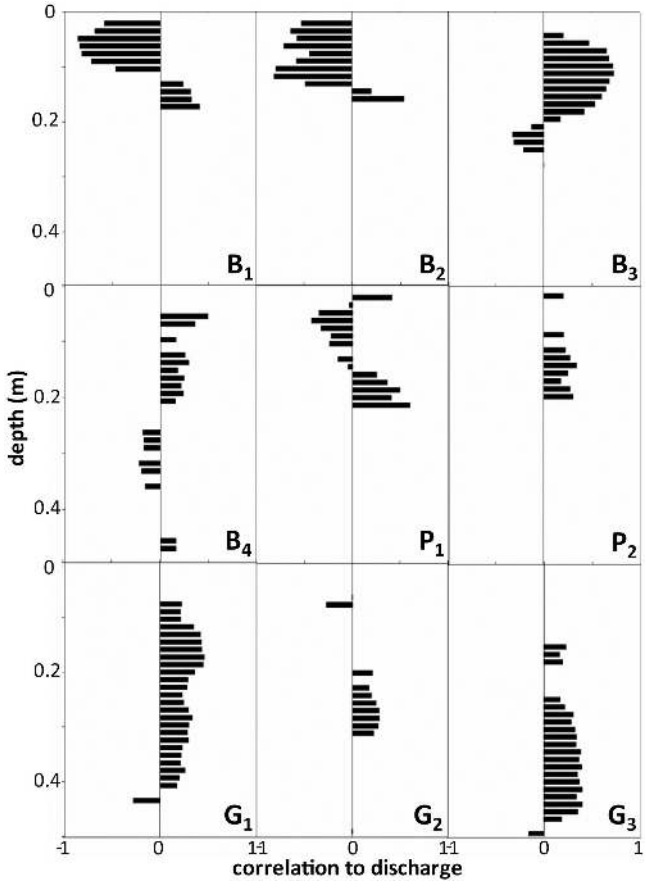

Figure 11. The correlations between vertical flux over the study period (every 2 h) and discharge with significance greater than $p = 0.01$, plotted by depth for each HRTS. Significant positive correlation was generally observed at the glides (G_1, G_2, and G_3) and lower bar sites (B_3 and B_4), while the upstream bar locations (B_1 and B_2) had strong negative correlations within the upper 0.1 m of the bed, indicating increased seepage as flow decreased.

4. Discussion

4.1. High-Resolution Temperature Data and Vertical Flux Method

[33] The raw high-resolution temperature data revealed many interesting and valuable attributes of the subsurface condition upstream of beaver dams, even before the 1-D flux calculation was applied. Attenuation of the diurnal signal amplitude showed significant variation between the various HRTS locations. The upstream bar (B_1, B_2) and pool (P_1, P_2) profiles had heat transport that was dominated by conduction as seen by the strong dampening of the signal amplitude with depth. Conversely, the glides (G_1, G_2, G_3) and downstream bar locations (B_3, B_4) had strong initial signal transmission because of high advective hyporheic transport. In addition to the inter-HRTS location variability, the amplitude of the diurnal temperature signal did not decline uniformly with depth at any profile (Figure 6), indicating that advection of heat and associated vertical hyporheic flux was not uniform with depth. Without prior knowledge of the flow system at each profile location, traditional deployment of fewer fixed-depth temperature sensors [e.g., *Hatch et al.*, 2006; *Keery et al.*, 2007; *Fanelli and Lautz*, 2008; *Anibas et al.*, 2009] would have been inadequate to resolve the change in temperature amplitude and associated changes in vertical flux. Additionally, the ideal analysis window spacing at our profiles was not uniform, so deployment of fixed-depth sensors would have likely resulted in poor resolution of flux at some locations. The Figure 3 inset shows how using a large vertical sensor window in a variable oblique flow system would obscure the transition to horizontal flux with depth, and the necessity for multiple window sizes. Fundamentally, using the high spatial resolution temperature data, combined with flexible analysis window spacing, is beneficial when

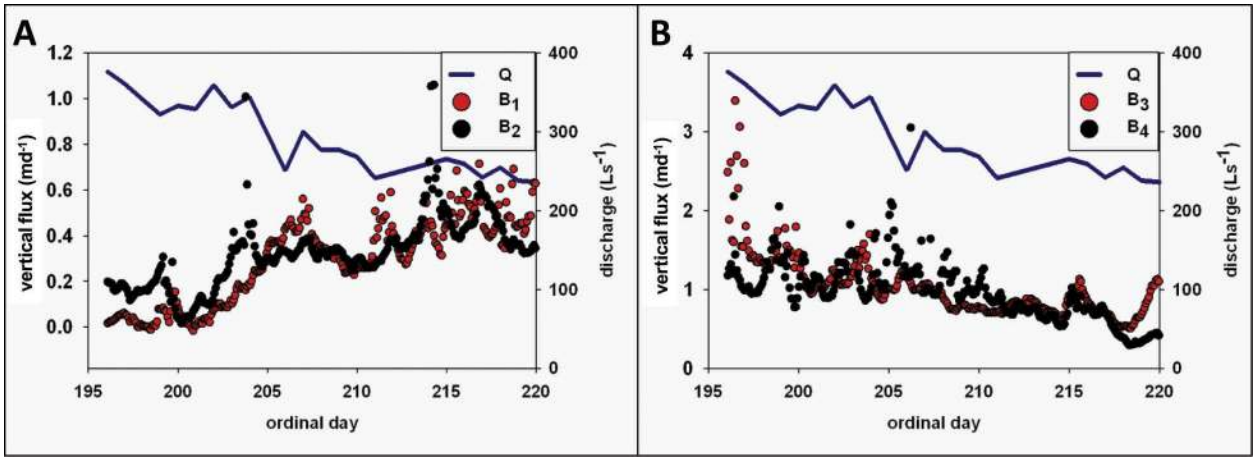

Figure 12. The patterns of vertical flux at similar shallow depths (0.05–0.1 m) at the bar locations that showed (a) strong positive correlation (B_3 of −0.72, B_4 of −0.49) or (b) strong negative correlation (B_1 of −0.86, B_2 of −0.57) to stream discharge through time. The flux at B_3 and B_4 was of much higher magnitude initially, but by the end of the period all locations had similar values. The shallow hyporheic exchange at the bar locations farther from the dam (B_1, B_2) was likely driven by hydraulic pumping, which may have been enhanced as stage dropped and flow became more turbulent. Conversely, B_3 and B_4 were close to their respective dam where the channel was wide; therefore, flux was probably influenced by the reduction in stream stage and velocity, which would have reduced pressure head on the streambed.

estimating flux patterns that are variable in space and time, because of the sensitivity of flux resolution to Δz [*Hatch et al.*, 2006]. By combining six analysis window spacings, optimized to the range in flux observed along each profile, locations of high flux were quantified while still resolving transitions to low flux at depth with high spatial resolution. The resulting flux matrices effectively integrate the benefits of a range of analysis window spacings (Figure 8).

[34] Before any reasonable discussion of variable vertical flux can be made, it is crucial to understand how flux could vary along a vertical profile, particularly when using a 1-D flux model. Flux is a volume, so although in true 1-D flow pore water velocities can vary with effective porosity, the volume of water passing through a medium in 1-D at one time cannot. This may appear to create a mass balance problem when vertical flux patterns vary along a vertical profile; however, in shallow hyporheic flow cells, as we may expect around both bed forms and steps in the water surface profile, a vertical profile will ultimately cut across a series of different of flow paths each with their own flux mass balance (Figure 3). These types of flow cells have been predicted and documented by a multitude of hyporheic research [e.g., *Harvey and Bencala*, 1993; *Kasahara and Wondzell*, 2003; *Cardenas et al.*, 2004, *Gooseff et al.*, 2006; *Lautz and Siegel*, 2006; *Buffington and Tonina*, 2009]. The variability in hyporheic flow path magnitude, length and residence time has been considered as an explanation for why hyporheic exchange has power law behavior [*Haggerty et al.*, 2002; *Gooseff et al.*, 2003; *Cardenas et al.*, 2008]. The shallow hyporheic flow patterns conceptualized by *Buffington and Tonina* [2009] show that in step pool sequences, analogous to beaver dams, flow paths upstream of the step are initially vertical but transition to the horizontal with depth, while deeper, long flow paths are almost completely horizontal. This transition is caused by head pressures along a flow path equalizing with depth to the downstream discharge point, or the presence of a horizontal layer of low permeability. This concept is likely valid for the Cherry Creek reach which showed no change in net streamflow over the beaver dams, and therefore no diverging flow at depth as may be expected in the groundwater mounding below losing streams. Additionally, the presence of cold water at depth at the pool locations indicated the shallow hyporheic flow cells are underlain by deeper down-valley flow paths. This type of strong shallow vertical hyporheic flux which diminishes with depth has recently been observed in streams using various heat tracing methods [*Vogt et al.*, 2010; *Jensen and Engesgaard*, 2011], and likely results from the transition to oblique then horizontal flow paths down the profile.

[35] For this setting a spectrum of hyporheic flow paths along a vertical profile will likely transition to the horizontal plane with depth, therefore the assumption must be made that the 1-D flux model used for this analysis is valid for determining the vertical component of oblique flow. For example, *Lautz* [2010] showed this assumption to be theoretically true through a numerical modeling exercise using VS2DH [*Healy and Ronan*, 1996]. The author's results indicate that the vertical component of the flow vector at any point within a two-dimensional flow field is well described by the 1-D model. Absolute errors of vertical flux estimates are greater than 50% when flow is dominated by the horizontal component (v_z:v_x < 0.31), in part because the values of v_z are so small. Despite this difference, the 1-D model estimates of flux are much more representative of the vertical velocity vector, rather than the total or horizontal velocity vectors. Consequently, the high-resolution temperature data gives us both a method to quantify the

vertical component of hyporheic flux across a spectrum of flow paths, and to determine the depth to which shallow hyporheic flow has any vertical component. In this way the high-resolution data set is novel, as it allows us to move beyond the purely conceptual and model domains, and quantitatively evaluate a spectrum of vertical hyporheic flow vectors measured in the field. It should also be noted that the A_r analytical method was chosen for this investigation because it is least affected by nonideal field conditions [*Hatch et al.*, 2006; *Lautz*, 2010]. Models based on the phase shift of the diurnal signal with depth presented by both *Hatch et al.* [2006] and *Keery et al.* [2007] were also used for this data set and erratically produced unreasonably high results (e.g., many estimates of flux greater than 10 m d^{-1} for all profiles).

4.2. High-Resolution Vertical Flux Patterns Above Beaver Dams

[36] The median flux with depth showed patterns that indicated both streambed morphology and proximity to the dam exerted strong controls on hyporheic exchange upstream of the beaver dams. The bar locations farthest away from the dam (B_1 and B_2) were likely dominated by "pumping model" type exchange [e.g., *Elliot and Brooks*, 1997] and showed shallow (less than 0.12 m) and modest (less than 0.4 m d^{-1}) vertical flux along hyporheic flow paths. The pools (P_1 and P_2) had a similar flux condition to that of the upstream bar sites (B_1 and B_2), even though the pools were much closer to their respective dams, and in close proximity to glide profiles that showed significant flux. The collection of fine particles in the pools may have reduced hydraulic conductivity and subsequent flux into the subsurface.

[37] Despite this, vertical flux through pool bottoms measured in this study was significantly higher than in previous investigations, which found very modest seepage (approximately 0.05 m d^{-1}) of stream water through pools, despite large negative hydraulic head gradients [*Fanelli and Lautz*, 2008; *Lautz et al.*, 2010]. The combination of low flux and high gradients in these studies was attributed to the collection of fines within the pools that may have greatly reduced hydraulic conductivity and impaired hyporheic flux. This condition likely played a lesser role at the Cherry Creek pools, as only a surficial layer of silt and clay was observed at those locations, and much of this fine grained material had been scoured out during the extremely high snowmelt flows that occurred in late spring, immediately preceding this work. Another reason why pool locations had a reduced vertical flux component compared to the neighboring glide locations at Cherry Creek is that the bottom of the pools were at a lower elevation than the surrounding bed (Figure 2), and even below the downstream water surface at Dam 2. In such a configuration, pressure head would change rapidly with depth into the streambed and we may expect any hyporheic flux through the pool bottom to be dominated by the horizontal component, which we cannot distinguish from low total flux using this method.

[38] We found much higher flux in the upper bed at the glides (G_1, G_2, and G_3) and lower two bar locations (B_3 and B_4) of 1.6 to 0.9 m d^{-1}, exceeding fluxes determined for similar depths at small downstream beaver and anthropogenic dams evaluated in previous investigations using lower resolution temperature modeling (less than 0.5 m d^{-1}) [*Lautz et al.*, 2010; *Fanelli and Lautz*, 2008] (Figures 8 and 9). Our vertical flux values are more similar to the lower end of flux rates found using high-resolution temperature methods in a losing section of a large gravel bed river [*Vogt et al.*, 2010]. These results indicate that a significant volume of stream water is moving into the subsurface above beaver dams at Cherry Creek, but this infiltration is patchy and found generally at glides and sediment bars close to dams. Both of these morphological units were observed to have coarser-grained sediments than the bottoms of pools, and the pressure head along glides should also contain a significant velocity component that would add to the elevation head gradient caused by the dam alone. The B_4 profile was located very close to the estimated edge of a glide and had particularly high flux and the most temporal anomalies, often showing increasing flux with depth. Stream bar deposits are known to have heterogeneous layers [*Weissmann and Fogg*, 1999], potentially creating highly oblique flux conduits at depth. This could produce zones of incalculable flux, yielding noisy or bare zones in the flux matrix as seen along this profile.

[39] As a common characteristic, similar magnitude fluxes were found at these locations for both sized dams, suggesting that once a threshold in water surface step is exceed, flux rates into the bed are limited by the general hydraulic conductivity of the sediments. High vertical flux zones at both dams also had similar transitions to horizontal flux with depth by approximately 0.5 m caused by head equilibration with depth and potentially the presence of confining layers. *Lautz et al.* [2006] predicted similar shallow flow cells (less than 1 m in depth) using numerical models, and concluded they likely dominate the biogeochemical processing capability of the hyporheic flow observed around beaver dams.

[40] For several of the low-flux sites there was an apparent shift to upwelling at depth (Figure 9). This scenario was unlikely on the basis of any reasonable physical process, so a Monte Carlo uncertainty analysis was performed over a reasonable range of sediment thermal properties to determine if the estimated negative flux was significantly different from zero (Table 2). The results of the analysis indicated uncertainty was at a minimum when vertical flux values were approximately 0.4 m d^{-1} (Figure 10), and increased as flux diminished and switched to negative through time at the 0.15 m HRTS B_3 location. This yielded an uncertainty range of ± 0.1 m d^{-1} around a zero flux estimate, indicating that the reversal to negative flux values at depth determined for the bar and pool locations were significant on the basis of streambed thermal property uncertainty alone. This is interesting because for many of these depths the diurnal temperature amplitude was still discernable from instrument noise (0.3°C–0.7°C), although at these depths there were higher signal to noise ratios and presumably lower confidence in flux estimates as a result. We cannot rule out that the observed upwelling at depth was valid, potentially caused by horizontal flow encountering clay lenses and being forced upward. More likely the stronger thermal gradients observed with depth at the pool and bar locations may have contributed to error using the 1-D model at depth there, as the presence of a thermal gradient, which

violates model assumptions, has been found to affect flux calculations especially under low vertical flow conditions [*Lautz*, 2010].

[41] The Cl^- tracer served to support the interpretation that the streambed profiles in Cherry Creek had hydraulic connection to the stream and showed varied rates of hyporheic flux, and is in concordance with earlier work that has shown good agreement between solute and thermal tracers [*Constantz et al.*, 2003]. The relatively high flux rates at glides, as determined through heat transport modeling, were supported by the high percentage of surface water at these locations, based on Cl^- enrichment, and the minimum median flux estimates based on the tracer arrival time, which were 0.81 m d^{-1} for the 0.15 m depth at all glide locations. The tracer-derived flux estimates are a minimum because of low temporal sampling resolution, and because the Cl^- flux estimates were made assuming pure vertical connection of all points to the surface; any longer, oblique flow path would result in a higher flux estimate using the tracer data. The low-flux temperature profiles were also generally well supported by the Cl^- data.

4.3. Temporal Evaluation of Flux Patterns

[42] Significant positive correlations were found between falling stream discharge and temporal changes in flux at the glides and downstream bar locations (B_3 and B_4) at intermediate to deep profile depths (Figure 11). As discharge decreased over the period of observation, so did stage and velocity, all of which may serve to reduce pressure head along the bed, and in turn reduce vertical flux with depth at these locations. In contrast, however, the upstream bar and pool locations (B_1, B_2, and P_1) unexpectedly showed significant increase in shallow vertical flux with decreasing discharge. A comparison can be made between the downstream bars close to the dam (B_3, B_4) and the upstream bars farther back from the dam (B_1, B_2) at similar depths, which show opposite correlations with stream discharge (Figure 12). The shallow hyporheic exchange at the bar locations far from the dam were likely driven though hydraulic pumping over the bar [*Elliot and Brooks*, 1997]. Flow over the upstream bars became noticeably more turbulent as stage dropped and the dam exerted less control over the stream profile there, a condition that did not occur over the downstream bar which was closer to the dam and where the stream was much wider (Figure 2a). The pressure which forces hyporheic interstitial flow may be increased by a transition from laminar to turbulent flow, enhancing exchange between the stream and subsurface through time. *Cao et al.* [2003], who investigated the "pool-riffle reversal hypothesis" with a two-dimensional numerical model, showed that as stage falls, bed shear stress and the Froude number may peak at the riffle (bar) tail, with a secondary peak at the adjacent pool head. As the only HRTS profiles which showed significant increase in shallow hyporheic flux were found at these morphologic locations, the bar tail (B_1, B_2) showing the largest increase and the pool head (P_1) showing modest increase, our field data may support these modeled dynamics. These patterns offer more evidence of the complicated spatial and temporal nature of hyporheic exchange, and could only have been captured at high data resolution in both regards.

4.4. Benefits of Fiber-Optic High-Resolution Temperature Sensors

[43] We have shown that the high-resolution temperature records that were collected with these custom sensors provided the necessary versatility to optimize quantitative flux analysis. As vertical hyporheic flux was shown to vary by morphology, distance from the dams, and through time, it would have been very difficult to a priori predict appropriate analysis window spacings using individual temperature loggers. The resulting data set would be inherently less precise, and the complexity of vertical flux patterns shown across a spectrum of hyporheic flow paths would not be well described. Precision in flux estimates may be particularly important when scaling up, such as determining total hyporheic flux at the reach scale using bed temperature as a proxy to flux rating curves [e.g., *Conant*, 2004]. If the initial vertical flux across the sediment water interface is not well quantified because of inappropriate analysis window spacing, these errors will be propagated throughout the interpolation process.

[44] Fiber-optic systems do have significant overhead in terms of monetary cost and logistical setup. Vertical "stacks" of many individual loggers could theoretically be used to provide analogous resolution to the fiber-optic HRTS, but they would all have to be individually calibrated and adjusted for differential instrument drift over the measurement period. In contrast, the entire nine profile DTS system collected synchronized temperature measurements and was kept calibrated for drift using one single record and procedure. This is extremely important when applying the 1-D flux model, as relative temperature accuracy is more important than absolute accuracy, e.g., modeled fluxes must be based on temperature record differences between depths resulting from physical processes rather than instrument error or offset. Although many individual loggers have higher precision than the DTS system used at Cherry Creek, the system parameters could have been reasonably adjusted to yield much better HRTS precision as has recently been shown by *Suárez et al.* [2011]. Finally, although temperature precision was relatively coarse (0.2°C), the method still performed well despite a very modest input signal (amplitude of 0.6°C–1.9°C) associated with high stream discharge and cold base flow. Many systems of interest would have larger diurnal amplitude swings during summer recession, even large rivers [e.g., *Constantz et al.*, 1994; *Vogt et al.*, 2010]. Moving forward, the spatially distributed temperature data collected with HRTS may be particularly useful to inform 2-D and 3-D numerical models (e.g., SUTRA, FLOW 3-D) which can be used to describe the total vector of oblique hyporheic flow.

[45] Managing the shear amount of data produced by high-resolution temperature monitoring systems can be challenging. Fortunately, programs are available for software such as MATLAB which can automate and streamline these processes significantly. We utilized the program VFLUX [*Gordon et al.*, 2012] to seamlessly integrate many existing data manipulation and signal processing tools to perform many complex processes on large data sets quickly and cleanly. Over 100,000 individual flux measurements were generated from pure diurnal signals (Figure 5a) extracted from the original temperature records for each

profile above Cherry Creek beaver dams. This kind of computational efficiency allowed us the flexibility to use the high-resolution records to their greatest potential. This flexibility included integration of multiple-sized sliding analysis windows that allowed us to optimize the evaluation of vertical flux which was highly variable with depth along vertical profiles.

5. Conclusions

[46] The purpose of this project was to use high-resolution temperature data to investigate the complicated hyporheic exchange dynamics observed around beaver dams, and to evaluate the feasibility and benefits of using multiple simultaneous fiber-optic HRTS over an extended period of time in the stream environment. The high-resolution temperature records provided a rich picture of flux through the streambed with depth through time, and similar patterns of diurnal signal transport were observed by general morphologic unit above two dams of varied size. The attenuation of the diurnal signal was used to quantitatively describe the vertical component of hyporheic flux from the stream into the subsurface using a 1-D flux model. This flux was patchy with evident "hot spots" of seepage near the dams though glides and bars, and more modest shallow flux through pools and bar locations farther upstream from the dams. Because hyporheic flux is fundamentally driven by streambed pressure and resisted by streambed hydraulic conductivity and competing groundwater inflow, the different observed flux patterns resulted both from the proximity to the dam step and from bed form heterogeneity. Specifically, shallow vertical flux at the glides and two close bar locations was 1.6 to 0.9 m d^{-1}, while shallow vertical flux at the upstream bars and pools was generally less than 0.3 m d^{-1}. These general patterns of flux were supported with conservative transport of Cl^- injected into the stream. All profiles showed a transition to horizontal flow with depth across a spectrum of hyporheic flow paths, with a penetration of vertical flux to approximately 0.45 m at glides and close bars and only approximately 0.12 m at pools and upstream bars. Finally, the upstream bars showed increasing flux with falling discharge over the month, which may be due to pumping model type exchange, while the other bar locations showed reduced flux with time, which may be due to decreasing head gradients over the beaver dams with decreasing stage.

[47] The HRTS design and installation was successful, with strong signal transmission allowing the system to be run in double-ended mode which aided in calibration. As all HRTS were run inline off the same unit, all data were on the same time step, and could all be adjusted simultaneously for instrument drift over the extended data collection period. The high-resolution temperature records allowed us to optimize the analysis window spacings to flux magnitude, which was highly variable in space. The fiber-optic HRTS is a valuable emerging tool, which can be used to describe hyporheic flow dynamics at high-resolution across a spectrum of flow paths. These sensors are an important addition to emerging geophysical and analytical methods which are moving our descriptions of the heterogeneous hyporheic zone beyond the point scale, to a more useful understanding integrated through space and time.

[48] **Acknowledgments.** We thank The Nature Conservancy of Wyoming for site access and logistical support. Timothy Daniluk, Dana Scott, Ricardo Gonzalez, and Dennis Lemke along with Suki Smaglick and several of her students from Central Wyoming Community College were instrumental in field assistance. This material is based upon work supported by the National Science Foundation under grant EAR-0901480. Any opinions, findings, and conclusions or recommendations expressed in this material are those of the authors and do not necessarily reflect the views of the National Science Foundation.

References

Anderson, M. P. (2005), Heat as a ground water tracer, *Ground Water*, *43*(6), 951–968.

Anibas, C., J. H. Fleckenstein, N. Volze, K. Buis, R. Verhoeven, P. Meire, and O. Batelaan (2009), Transient or steady-state? Using vertical temperature profiles to quantify groundwater–surface water exchange, *Hydrol. Processes*, *23*, 2165–2177, doi:10.1002/hyp.7289.

Briggs, M. A., L. K. Lautz, and J. M. McKenzie (2011), A comparison of distributed temperature sensing to traditional methods of evaluating groundwater inflows to streams, *Hydrol. Proc.*, *25*, Abstract 8200, doi:10.1002/hyp.8200.

Buffington, J. M., and D. Tonina (2009), Hyporheic exchange in mountain rivers II: Effects of channel morphology on mechanics, scales, and rates of exchange, *Geogr. Compass*, *3*(3), 1038–1062.

Cao, Z., P. A. Carling, and R. Oakley (2003), Flow reversal over a natural pool-riffle sequence: A computational study, *Earth Surf. Processes Landforms*, *28*, 689–705, doi:10.1002/esp.466.

Cardenas, M. B., J. L. Wilson, and V. A. Zlotnik (2004), Impact of heterogeneity, bed forms, and stream curvature on subsurface hyporheic exchange, *Water Resour. Res.*, *40*, W08307, doi:10.1029/2004WR003008.

Cardenas, M. B., J. L. Wilson, and R. Haggerty (2008), Residence time of bedform-driven hyporheic exchange, *Adv. Water Resour.*, *31*, 1382–1386, doi:10.1016/j.advwatres.2008.07.006.

Cirpka, O. A., M. N. Fienen, M. Hofer, E. Hoehn, A. Tessarini, R. Kipfer, and P. K. Kitanidis (2007), Analyzing bank filtration by deconvoluting time series of electric conductivity, *Ground Water*, *45*(3), 318–328.

Conant, B. (2004), Delineating and quantifying ground water discharge zones using streambed temperatures, *Ground Water*, *42*(2), 243–257.

Constantz, J. (2008), Heat as a tracer to determine streambed water exchanges, *Water Resour. Res.*, *44*, W00D10, doi:10.1029/2008WR006996.

Constantz, J., and C. L. Thomas (1996), The use of streambed temperature profiles to estimate the depth, duration, and rate of percolation beneath arroyos, *Water Resour. Res.*, *32*(12), 3597–3602.

Constantz, J., C. Thomas, and G. Zellweger (1994), Influence of diurnal variations in stream temperature on streamflow loss and groundwater recharge, *Water Resour. Res.*, *30*(12), 3253–3264.

Constantz, J., M. H. Cox, and G. W. Su (2003), Comparison of heat and bromide as ground water tracers near streams, *Ground Water*, *41*(5), 647–656.

Dakin, J. P., D. J. Pratt, G. W. Bibby, and J. N. Ross (1985), Distributed optical fiber Raman temperature sensor using a semiconductor light-source and detector, *Electron. Lett.*, *21*(13), 569–570.

Elliott, A. H., and N. H. Brooks (1997), Transfer of nonsorbing solutes to a streambed with bed forms: Theory, *Water Resour. Res.*, *33*(1), 123–136.

Fanelli, R. M., and L. K. Lautz (2008), Patterns of water, heat, and solute flux through streambeds around small dams, *Ground Water*, *46*(5), 671–687.

Gooseff, M. N., S. M. Wondzell, R. Hagerty, and J. Anderson (2003), Comparing transient storage modeling and residence time distribution (RTD) analysis in geomorphologically varied reaches in the Lookout Creek basin, Oregon, USA, *Adv. Water Resour.*, *26*(9), 925–937, doi:10.1016/S0309-1708(03)00105-2.

Gooseff, M. N., J. K. Anderson, S. M. Wondzell, J. LaNier, and R. Haggerty (2006), A modeling study of hyporheic exchange pattern and the sequence, size, and spacing of stream bedforms in mountain stream networks, Oregon, USA, *Hydrol. Processes*, *20*(11), 2443–2457.

Gooseff, M. N., R. O. Hall Jr., and J. L. Tank (2007), Relating transient storage to channel complexity in streams of varying land use in Jackson Hole, Wyoming, *Water Resour. Res.*, *43*, W01417, doi:10.1029/2005WR004626.

Gordon, R. P., L. K. Lautz, M. A. Briggs, and J. M. McKenzie (2012), Automated calculation of vertical pore-water flux from field temperature time series using the VFLUX method and computer program, *J. Hydrol.*, doi:10.1016/j.jhydrol.2011.11.053, in press.

Goto, S., M. Yamano, and M. Kinoshita (2005), Thermal response of sediment with vertical fluid flow to periodic temperature variation at the surface, *J. Geophys. Res. 110*, B01106, doi:10.1029/2004JB003419.

Haggerty, R., S. M. Wondzell, and M. A. Johnson (2002), Power-law residence time distribution in the hyporheic zone of a 2nd-order mountain stream, *Geophys. Res. Lett.*, *29*(13), 1640, doi:10.1029/2002GL014743.

Harvey, J. W., and K. E. Bencala (1993), The effects of streambed topography on surface-subsurface water exchange in mountain catchments, *Water Resour. Res.*, *29*(1), 89–98.

Harvey, J. W., and B. J. Wagner (2000), Quantifying hydrologic interactions between streams and their subsurface hyporheic zones, in *Streams and Groundwaters*, edited by J. B. Jones and P. J. Mulholland, pp. 9–10, Academic, San Diego, Calif.

Harvey, J. W., J. E. Saiers, and J. T. Newlin (2005), Solute transport and storage mechanisms in wetlands of the Everglades, south Florida, *Water Resour. Res.*, *41*, W05009, doi:10.1029/2004WR003507.

Hatch, C. E., A. T. Fisher, J. S. Revenaugh, J. Constantz, and C. Ruehl (2006), Quantifying surface water–groundwater interactions using time series analysis of streambed thermal records: Method development, *Water Resour. Res.*, *42*, W10410, doi:10.1029/2005WR004787.

Healy, R. W., and A. D. Ronan (1996), Documentation of computer program VS2DH for simulation of energy transport in variably saturated porous media—Modification of the U.S. Geological Survey's computer program VS2DT, *U.S. Geol. Surv. Water Resour. Invest. Rep., 96-4230*, 36 pp., U.S. Geological Survey: Branch of Information Services, Denver, CO, http://pubs.er.usgs.gov/publication/wri964230.

Hester, E. T., and M. W. Doyle (2008), In-stream geomorphic structures as drivers of hyporheic exchange, *Water Resour. Res.*, *44*, W03417, doi:10.1029/2006WR005810.

Jensen, J. K., and P. Engesgaard (2011), Nonuniform groundwater discharge across a streambed: Heat as a tracer, *Vadose Zone J.*, *10*, 98–109, doi:10.2136/vzj2010.0005.

Jin, L., D. I. Siegel, L. K. Lautz, and M. H. Otz (2009), Transient storage and downstream solute transport in nested stream reaches affected by beaver dams, *Hydrol. Processes*, *23*, 2438–2449.

Kasahara, T., and S. M. Wondzell (2003), Geomorphic controls on hyporheic exchange flow in mountain streams, *Water Resour. Res.*, *39*(1), 1005, doi:10.1029/2002WR001386.

Keery, J., A. Binley, N. Crook, and J. W. N. Smith (2007), Temporal and spatial variability of groundwater-surface water fluxes: Development and application of an analytical method using temperature time series, *J. Hydrol.*, *336*(1–2), 1–16.

Lapham, W. W. (1989), Use of temperature profiles beneath streams to determine rates of vertical ground-water flow and vertical hydraulic conductivity, *U.S. Geol. Surv. Water Supply Pap.*, *2337*.

Lautz, L. K. (2010), Impacts of nonideal field conditions on vertical water velocity estimates from streambed temperature time series, *Water Resour. Res.*, *46*, W01509, doi:10.1029/2009WR007917.

Lautz, L. K., and D. I. Siegel (2006), Modeling surface and ground water mixing in the hyporheic zone using MODFLOW and MT3D, *Adv. Water Resour.*, *29*(11), 1618–1633.

Lautz, L. K., D. I. Siegel, and R. L. Bauer (2006), Impact of debris dams on hyporheic interaction along a semi-arid stream, *Hydrol. Processes*, *20*, 183–196.

Lautz, L. K., N. T. Kranes, and D. I. Siegel (2010), Heat tracing of heterogeneous hyporheic exchange adjacent to in-stream geomorphic features, *Hydrol. Processes*, *24*(21), 3074–3086, doi:10.1002/hyp.7723.

Lowry, C. S., J. F. Walker, R. J. Hunt, and M. P. Anderson (2007), Identifying spatial variability of groundwater discharge in a wetland stream using a distributed temperature sensor, *Water Resour. Res.*, *43*, W10408, doi:10.1029/2007WR006145.

Moffett, K. B., S. W. Tyler, T. Torgersen, M. Menon, J. S. Selker, and S. M. Gorelick (2008), Processes controlling the thermal regime of saltmarsh channel beds, *Environ. Sci. Technol.*, *42*(3), 671–676, doi:10.1021/es071309m.

Naiman, R. J., J. M. Melillo, and J. E. Hobbie (1986), Ecosystem alteration of boreal forest streams by beaver (*Castor canadensis*), *Ecology*, *67*, 1254–1269.

Pidlisecky, A., and R. Knight (2012), The use of wavelet analysis to derive infiltration rates from time-lapse 1D resistivity records, *Vadose Zone J.*, doi:10.2136/vzj2010.0049, in press.

Rau, G. C., M. S. Andersen, A. M. McCallum, and R. I. Acworth (2010), Analytical methods that use natural heat as a tracer to quantify surface water–groundwater exchange, evaluated using field temperature records, *Hydrogeol. J.*, *18*, 1093–1110, doi:10.1007/s10040-010-0586-0.

Schmidt, C., M. Martienssen, and E. Kalbus (2011), Influence of water flux and redox conditions on chlorobenzene concentrations in a contaminated streambed, *Hydrol. Processes*, *25*(2), 234–245, doi:10.1002/hyp.7839.

Selker, J. S., L. Thévenaz, H. Huwald, A. Mallet, W. Luxemburg, N. van de Giesen, M. Stejskal, J. Zeman, M. Westhoff, and M. B. Parlange (2006a), Distributed fiber-optic temperature sensing for hydrologic systems, *Water Resour. Res.*, *42*, W12202, doi:10.1029/2006WR005326.

Selker J. S., N. van de Giesen, M. Westhoff, W. Luxemburg, and M. B. Parlange (2006b), Fiber optics opens window on stream dynamics, *Geophys. Res. Lett.*, *33*, L24401, doi:10.1029/2006GL027979.

Stallman, R. W. (1965), Steady one-dimensional fluid flow in a semi-infinite porous medium with sinusoidal surface temperature, *J. Geophys. Res.*, *70*(12), 2821–2827.

Suárez, F., J. E. Aravena, M. B. Hausner, A. E. Childress, and S. W. Tyler (2011), Assessment of a vertical high-resolution distributed-temperature sensing system in a shallow thermohaline environment, *Hydrol. Earth Syst. Sci.*, *15*, 1081–1093, doi:10.5194/hess-15-1081-2011.

Triska, F. J., V. C. Kennedy, R. J. Avanzino, G. W. Zellweger, and K. E. Bencala (1989), Retention and transport of nutrients in a third-order stream in northwestern California: Hyporheic processes, *Ecology*, *70*, 1893–1905.

Tyler, S. W., J. S. Selker, M. B. Hausner, C. E. Hatch, T. Torgersen, C. E. Thodal, and S. G. Schladow (2009), Environmental temperature sensing using Raman spectra DTS fiber-optic methods, *Water Resour. Res.*, *45*, W00D23, doi:10.1029/2008WR007052.

Vogt, T., P. Schneider, L. Hahn-Woernle, and O. A. Cirpka (2010), Estimation of seepage rates in a losing stream by means of fiber-optic high-resolution vertical temperature profiling, *J. Hydrol.*, *380*(1–2), 154–164.

Vroblesky, D. A., and F. H. Chapelle (1994), Temporal and spatial changes of terminal electron-accepting processes in a petroleum hydrocarbon contaminated aquifer and the significance for contaminant biodegradation, *Water. Resour. Res.*, *30*, 1561–1570.

Ward, A. S., M. N. Gooseff, and K. Singha (2010), Imaging hyporheic zone solute transport using electrical resistivity, *Hydrol. Processes*, *24*(7), 948–952, doi:10.1016/j.advwatres.2010.05.008.

Weissmann, G. S., and G. E. Fogg (1999), Multi-scale alluvial fan heterogeneity modeled with transition probability geostatistics in a sequence stratigraphic framework, *J. Hydrol.*, *226*(1–2), 48–65.

Westhoff, M. C., H. H. G. Savenije, W. M. J. Luxemburg, G. S. Stelling, N. C. van de Giesen, J. S. Selker, L. Pfister, and S. Uhlenbrook (2007), A distributed stream temperature model using high resolution temperature observations, *Hydrol. Earth Syst. Sci.*, *11*(4), 1469–1480.

Young, P. C., D. J. Pedregal, and W. Tych (1999), Dynamic harmonic regression, *J. Forecast.*, *18*(6), 369–394.

Young, P. C., C. J. Taylor, W. Tych, D. J. Pegregal, and P. G. McKenna (2010), The Captain Toolbox, software, http://www.es.lancs.ac.uk/cres/captain, Cent. for Res. on Environ. Syst. and Stat., Lancaster Univ., U. K.

Zarnetske, J. P., R. Haggerty, S. M. Wondzell, and M. A. Baker (2011), Dynamics of nitrate production and removal as a function of residence time in the hyporheic zone, *J. Geophys. Res.*, *116*, G01025, doi:10.1029/2010JG001356.

M. A. Briggs, R. P. Gordon, D. K. Hare, and L. K. Lautz, Department of Earth Sciences, Syracuse University, 204 Heroy Geology Laboratory, Syracuse, NY 13244, USA. (martybriggs.1@gmail.com)

J. M. McKenzie, Department of Earth and Planetary Sciences, McGill University, 3450 University St., Montreal, QC H3A 2A7, Canada.